

Probing cosmic plasma with giant radio pulses

V. I. Kondratiev,^{1,2,3,*} M. V. Popov,^{1,**} V. A. Soglasnov,¹
Y. Y. Kovalev,^{1,4,5} N. Bartel,³ W. Cannon,³ and A. Yu. Novikov³

¹*Astro Space Center of the Lebedev Physical Institute, Profsoyuznaya 84/32, Moscow,
117997 Russia*

²*Department of Physics, West Virginia University, PO Box 6315, Morgantown, WV 26505, USA*

³*York University, Department of Physics and Astronomy, 4700 Keele Street, Toronto,
Ontario M3J 1P3 Canada*

⁴*National Radio Astronomy Observatory, P.O. Box 2, Green Bank, WV 24944, USA*

⁵*Max-Planck-Institut für Radioastronomie, Auf dem Hügel 69, 53121 Bonn, Germany*

VLBI observations of the Crab pulsar with the 64-m radio telescope at Kalyazin (Russia) and the 46-m radio telescope of the Algonquin Radio Observatory (Canada) at 2.2 GHz and single-dish observations of the millisecond pulsar B1937+21 with the GBT (USA) at 2.1 GHz were conducted to probe the interstellar medium and study the properties of giant pulses. The VLBI data were processed with a dedicated software correlator, which allowed us to obtain the visibility of single giant pulses. Two frequency scales of 50 and 450 kHz were found in the diffraction spectra of giant pulses from the Crab pulsar. The location of the scattering region was estimated to be close to the outer edge of the nebula. No correlation was found between the power spectra of giant pulses at left- and right-hand circular polarization. We explain this lack of correlation through the influence of the strong magnetic field on circularly polarized emission in the region close to the Crab pulsar.

Combining the measurement of the decorrelation bandwidth with that of the scattering time of giant pulses for B1937+21, we found three frequency scales of 1.7, 3.8, and 16.5 MHz. The scattering time of giant pulses of B1937+21 at 2.1 GHz was found to be 40 ± 4 ns. We obtained an upper limit of the intrinsic width of giant pulses from B1937+21 of less than 8 ns. The frequency dependences of the scattering times for the Crab pulsar and PSR B1937+21 were found to be different. They are characterized by exponents of -3.5 and -4.2 , respectively. We attribute the difference to the large influence of scattering in the Crab nebula.

1. INTRODUCTION

Pulsar radio emission on its way to Earth is affected by the turbulent interstellar medium (ISM) which is observed through dispersion, pulse and angular broadening, intensity scintillations, diffraction in radio spectra, and other effects. Given these effects it is very difficult to study the original properties of the unaffected emission. But, on the other hand, they are very useful to probe the ISM itself. The most encouraging probes to study the ISM seem to be giant radio pulses (GPs) due to their huge flux densities (up to tens of MJy), short durations (of order nanoseconds), and very high degree of polarization. Below we are studying the properties of the ISM with the GPs from the millisecond pulsar B1937+21 and the Crab pulsar. We have also used the influence of the ISM on regular pulsar emission to determine an upper limit on the intrinsic width of GPs.

2. OBSERVATIONS

In this paper we present a preliminary analysis of a) VLBI observations of the Crab pulsar with the 64-m radio telescope at Kalyazin (Russia) and the 46-m radio telescope of the Algonquin Radio Observatory (ARO, Canada) at 2244 MHz and b) single-dish observations of B1937+21 with the Robert C. Byrd Green Bank Telescope (GBT, USA) at 2.1 GHz.

VLBI observations of the Crab pulsar were conducted on July 19–20, 2005 with the S2 VLBI system [1] providing continuous recording in two 16-MHz bands. We recorded upper and lower sidebands (USB and LSB) at the central frequency of 2244 MHz at ARO where only one polarization channel (left circular) was available, and recorded only USB for both left- and right-hand circular polarization (LCP, RCP) at Kalyazin. Such configuration was used in order to overcome possible inconsistencies in the designation of polarization channels at the two observatories. Two observing sessions were carried out, each session lasting for about 3 hours with additional 10 minutes each at the start and the end of the session for observations of the continuum calibration source DA193.

Observations of the millisecond pulsar B1937+21 were done on June 7, 2005 with the GBT at a frequency of 2.1 GHz in both LCP and RCP with a time resolution of 8 ns. Four adjacent

* Electronic address: vlad@asc.rssi.ru

** Electronic address: mpopov@asc.rssi.ru

16-MHz channels (2052–2116 MHz) at each polarization were digitized simultaneously with 2-bit sampling at the Nyquist rate. The Mark5A data acquisition system was used for the first time in *single-dish* observations with the GBT [2]. This allowed us to obtain continuous and uniform recording for about 7.5 hours with a data rate of 512 Mbps. The quasar 3C286, the radio source 3C399.1, and the planetary nebula NGC 7027 were observed as well, for flux density and polarization calibration. The system temperature in all 8 separate frequency channels was about 23 K.

3. VLBI OBSERVATIONS OF GIANT PULSES FROM THE CRAB PULSAR

3.1. Peculiarities of the data reduction

In our observations we expected to find large sudden amplitude increases of the cross-correlation function (CCF) at short and random time intervals when GPs occurred. GPs have typical time scales of a few microseconds, and their peak flux densities can exceed a million Jy after dispersion removal. To provide dedispersion and allow for short integration we developed dedicated software for the following functions: time alignment of recorded signals, decoding of the 2-bit sampling with corrections for current bit statistics, predetection dedispersion, fringe compensation, calculation of the CCF via FFT, and postcorrelation analysis. The software is based on a geometric delay model, which we used in a form of the polynomial

$$\tau_g(t) = a + b(t - t_0) + c(t - t_0)^2 + d(t - t_0)^3 . \quad (1)$$

In our simple case of two radio telescopes, $\tau_g(t)$ represents the relative time delay with the time at the Kalyazin radio telescope used as a reference. The coefficients of the polynomial were calculated with the software “WinEra”, provided by the Institute of Applied Astronomy in St. Petersburg [3]. To obtain the fringe frequency we multiplied the signal recorded at ARO with the complex function $\exp(-j2\pi\nu_0\tau_g(t))$. In our case the residual phase delay can be written as

$$\phi_{12}(t) = 2\pi[\nu_0\Delta\tau_g(t) + \Delta\nu_0t + \phi_V(t)] , \quad (2)$$

where $\Delta\tau_g(t)$ is the residual delay due to an inaccurate knowledge of the source or radio telescope position; $\Delta\nu_0$ the difference between the LO-frequencies at the observatories; and $\phi_V(t)$ the phase delay produced by the atmosphere, ionosphere, and scattering medium.

The data reduction was conducted at the Astro Space Center (Moscow, Russia). The data from the S2 video tapes were copied to hard disk using the Radioastron Data Recorder Interface (RDR). The time delay compensation was implemented in two stages removing first integer and then fractional delays, the latter through phase correction of the spectrum together with dispersion removal. The dispersion smearing, τ_{DM} , over a 16-MHz band at a frequency of 2244 MHz for the used value of $\text{DM} = 56.737 \text{ pc cm}^{-3}$ [4] is equal to $660 \mu\text{s}$. The predetection dispersion removal technique [5] requires that the time interval, T , used for compensation must be longer than τ_{DM} . We used $T = 8192 \mu\text{s}$ (number of samples: $N=262,144$) for dedispersion and fringe compensation. The CCFs were computed via FFT (FX-correlator) on time arrays, ΔT , of $32 \mu\text{s}$ duration ($N=1024$). The normalized CCF magnitude was derived as $M_{\text{ccf}} = (\sqrt{R_{\text{ccf}}^2 + I_{\text{ccf}}^2})/(\sqrt{\text{acf}_1 \cdot \text{acf}_2})$, where R_{ccf} and I_{ccf} are, respectively, the real and imaginary components of the CCF, and acf_1 , acf_2 are the values of the autocorrelation functions (ACF) at zero-lag for the two observing sites for the given time interval ΔT . The expected value of the rms deviation of CCF magnitudes can be estimated as $\sigma_{\text{CCF}} = 1/\sqrt{N} = 0.031$. In our search for CCFs on GPs we used the threshold of $6\sigma = 0.186$ in a restricted range of time lags of $\pm 0.1\mu\text{s}$, and CCFs with magnitudes greater than the threshold were selected for postcorrelation analysis. The visibility amplitude was corrected for the signal-to-noise ratio (SNR) by multiplying it with the factor $R = \frac{\sigma_{\text{t1}}\sigma_{\text{t2}}}{\sqrt{((\sigma_{\text{t1}}^2 - \sigma_{\text{off1}}^2)(\sigma_{\text{t2}}^2 - \sigma_{\text{off2}}^2))}}$, where σ_{t1} and σ_{t2} are GP on-pulse rms deviations for a given ΔT and σ_{off1} and σ_{off2} are the equivalent values for the noise portion of the records. The visibility phase was determined as $\phi_{\text{V}} = \text{arctg}(I_{\text{ccf}}/R_{\text{ccf}})$ with I_{ccf} and R_{ccf} taken at the maximum magnitude of the CCF.

3.2. Scintillations of the visibility function

The scattering of the initially coherent electromagnetic radiation from a pulsar caused by the inhomogeneities of the cosmic plasma produces angular broadening of the source image, time smearing of individual pulses, and diffraction distortion of the radio spectrum. A simple model of a thin screen located midway between Earth and the pulsar provides the following relations [6, p. 91]: $\tau_{\text{sc}} = \theta_{\text{sc}}^2 D/4c$, and $2\pi\tau_{\text{sc}}\Delta f = 1$, where τ_{sc} is the time smearing parameter, θ_{sc} the angular diameter of the scattered image, D the distance to the pulsar, and Δf the decorrelation bandwidth. The maximum resolution of our two-element interferometer was equal to $\theta_I = \lambda/B = 4 \text{ mas}$ ($B=6750 \text{ km}$), while the angular diameter of the scattered

image corresponding to $\tau_{\text{sc}} = 200$ ns is estimated to be about 0.4 mas. Therefore, we did not expect to readily resolve the scattered image, but we hoped to relate certain effects of the scattering to the time and frequency behavior of the visibilities measured for the GPs.

First, the magnitudes of the visibilities for all strong GPs ($\text{SNR}_{\text{CCF}} > 10$), when corrected for finite SNR (factor R above), are close to 0.92 ± 0.05 . So, we did not detect any clear decorrelation caused by the diffraction pattern produced in the plane of observations by interstellar scattering. In fact, our observations are similar to "snapshot" observations, since we obtain essentially instant values of the visibility (formal integration time is $32 \mu\text{s}$). However, in the frequency domain, the integration was done over a total bandwidth of 16-MHz, covering many diffraction scintles in the spectrum. We will see below that at least two scales of diffraction scintles were found in the radio spectra with widths of about 50 and 450 kHz. Following Cordes et al. [7] one will find about $0.4B_{\text{tot}}/\Delta f$ scintles across a total band, B_{tot} . In our case the numbers are about 130 and 15 scintles for narrow and broad structures, respectively. Therefore, we are averaging in fact complex vectors of visibility over that number of scintles, and still have them coherent (no loss of correlation magnitude). This result is quite natural, since our two-element interferometer did not resolve the scattered disk.

Let us now consider the time behavior of the residual phase of the visibility presented in Figure 1 for the period of about an hour. At the beginning of the observing session one can see a constant residual phase with only relatively small random variations relative to the zero level with an rms deviation $\sigma \sim 0.5$ rad. This behavior continues during several minutes after an observing gap caused by troubleshooting of pointing at Kalyazin. Then there occurs a negative jump in phase followed by a linear drift at the rate of 0.042 rad/s. The reason of the drift may be the lock-on of the local oscillator system at one observing site with a relative inaccuracy of 3×10^{-12} .

The phase structure function $D_\phi(\tau) = \langle [\phi_V(t) - \phi_V(t + \tau)]^2 \rangle_\tau$ for the Crab pulsar is shown in Figure 2 (left) together with the phase structure function obtained for the continuum source DA193 observed at the beginning of the session. One can see that the phase structure functions for the pulsar and the continuum source are drastically different. The residual rms phase variations of the visibility function for DA193 are about 0.1 rad for short time intervals ($\tau < 1$ c) between measurements, and they are saturated at long time intervals ($\tau > 1$ min) at a level of about 0.4 rad in rms. We attribute these variations to the effects of

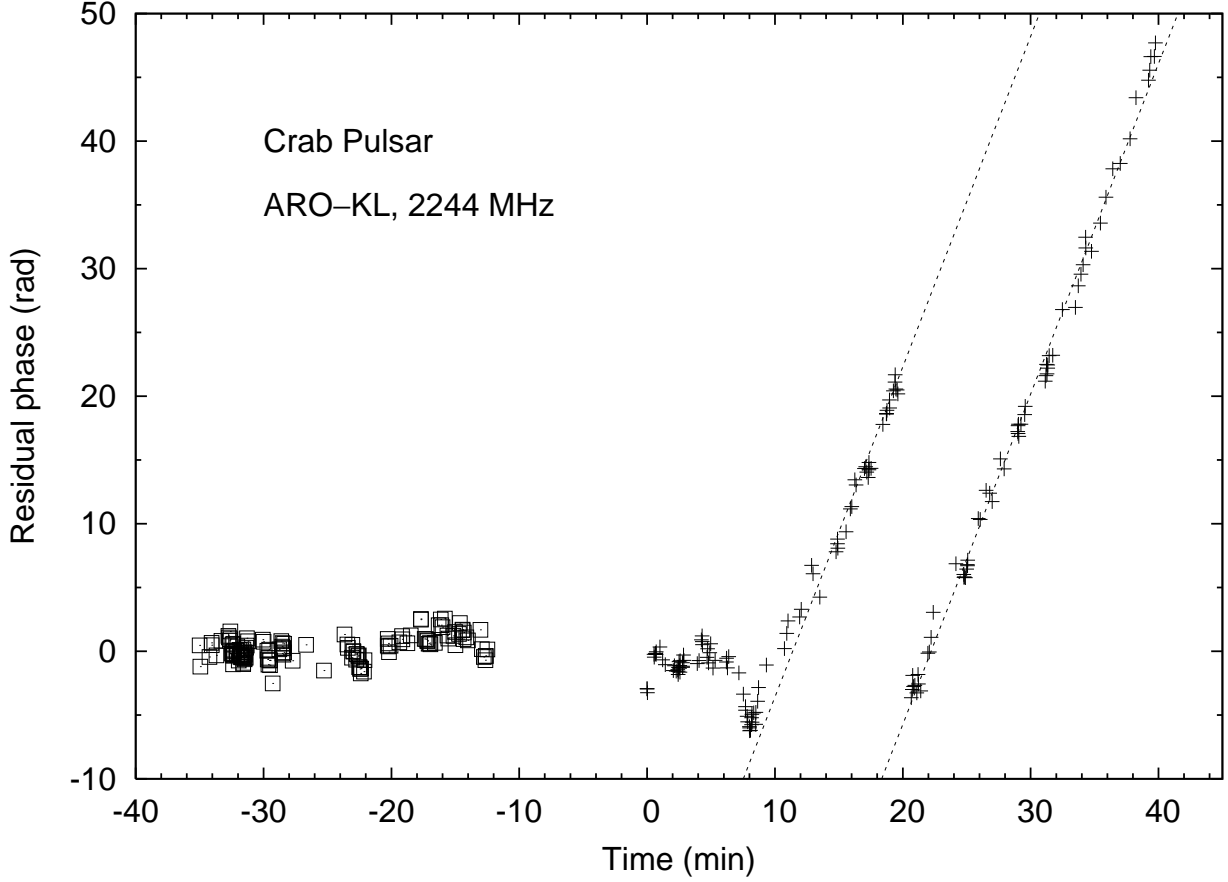


Figure 1. The residual phase of visibility in a time interval of about an hour during VLBI observations of the Crab pulsar between ARO and Kalyazin (KL) at 2244 MHz. Squares and pluses represent the residual phase in radians before and after the gap caused by the pointing problems at Kalyazin. Dashed lines represent the linear drift in phase at the rate of 0.042 rad/s due to the lock-on of LO at one of the observatories.

the atmosphere and ionosphere. The residual rms phase variations of the visibility function for the Crab pulsar are about 5 times larger (≈ 0.5 rad) than those caused by the atmosphere and the ionosphere, even for the shortest time intervals (there were 73 GPs separated by less than 1 second in time). Since we do not apply any time averaging of visibility, the observed phase variations can be interpreted as random angular displacements of the point source in the range restricted by the scattering disk with diameter θ_{sc} . Using relation (2) one can convert the phase variations to geometrical delay variations via $\Delta\tau_g = \Delta\phi_V/2\pi\nu_0$, thus obtaining $\Delta\tau_g = 3.5 \times 10^{-11}$ c. On the other hand, we can convert such variations in

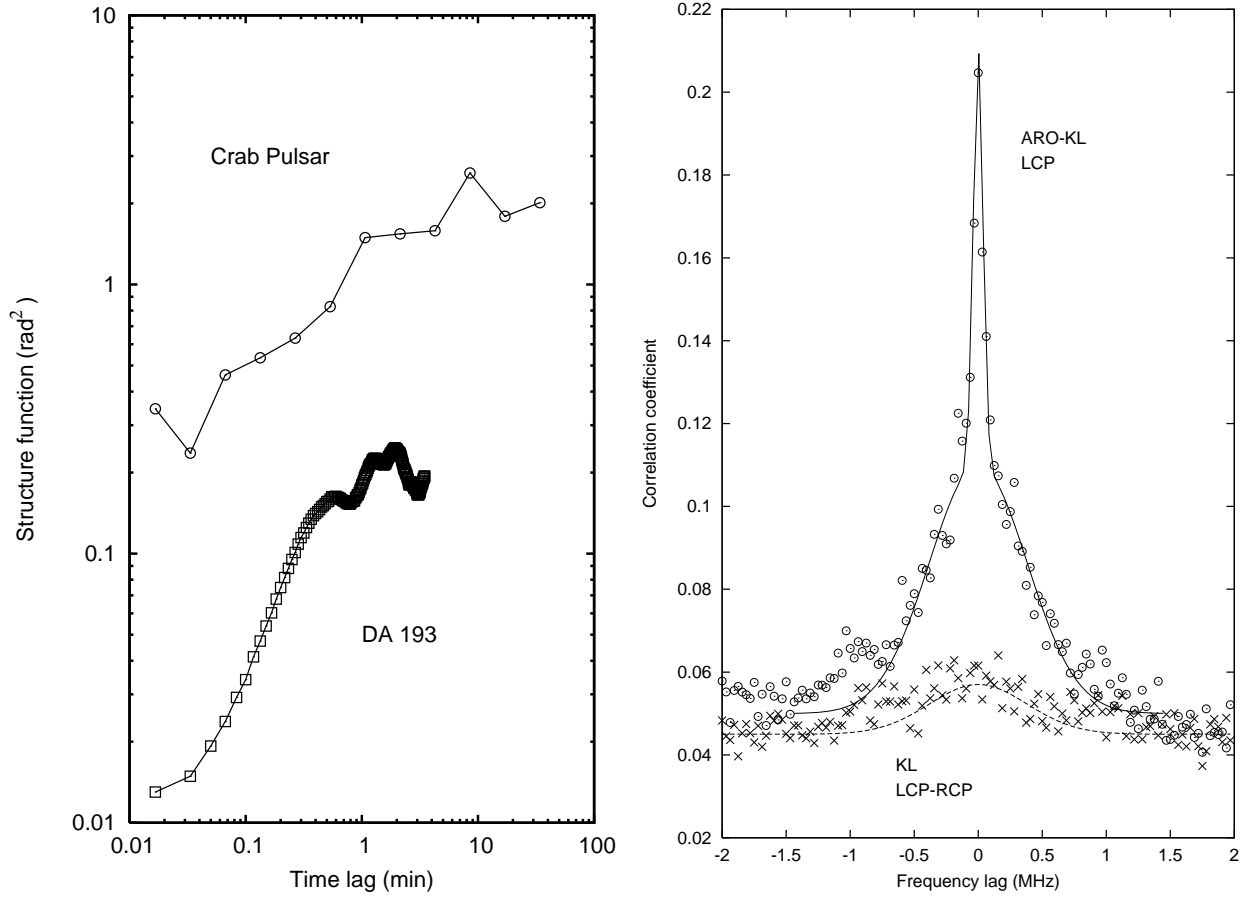


Figure 2. **Left.** Phase structure function of visibility phase variations for the Crab pulsar (circles) and quasar DA193 (squares). **Right.** The average CCF between power spectra of GPs recorded at LCP at Kalyazin and ARO (circles), and the average CCF between power spectra of the same GPs recorded at Kalyazin at LCP and RCP (crosses). The solid line is the approximation of the average CCF with two gaussians having half-widths of 50 and 450 kHz. The dashed line indicates the broad feature of 450 kHz marginally seen on the average CCF between power spectra of GPs recorded at Kalyazin at LCP and RCP. The frequency resolution is 30 kHz.

τ_g to a corresponding scattering diameter $\Delta\theta_\tau$ via the relation [8, p. 376]

$$\frac{\Delta\tau_g}{\Delta\theta_\tau} = \frac{B}{c} \cos \theta ,$$

where θ is the angle between the source vector and the plane perpendicular to the baseline. For the part of the observing session under consideration, θ was equal to 15° , resulting in a projected baseline length of $B_p = B \cos \theta = 6500$ km. Finally, we got an estimate for the scattering diameter of $\Delta\theta_\tau = (c\Delta\tau_g)/B_p = 1.5 \times 10^{-9}$ rad = 0.3 mas. We would like to emphasize that the technique of "phase self referencing" used above provides at least a

tenfold better sensitivity of estimating the scattering diameter than the formal resolving power of our two-element interferometer.

With the $\Delta\theta_\tau$ estimate in hand we can get additional information on the location of the scattering region (screen). Following the technique used by [9] in their analysis of the speckle hologram of the scattering material along the line of sight to the Vela pulsar, we get

$$\frac{dD}{D-d} = \frac{2.64 \times 10^{11}}{\Delta f (\Delta\theta_\tau)^2} .$$

Here D is the distance to the pulsar ($D = 2$ kpc), d the distance from the observer to the scattering screen, and Δf the decorrelation bandwidth. We will show below that the radio spectrum of GPs indicates two scales of diffraction pattern with $\Delta f_n = 50 \pm 10$ kHz (narrow feature), and $\Delta f_b = 450 \pm 10$ kHz (broad feature), with both structures having approximately equal modulation indices (see Figure 2, right). It appears reasonable to suggest that the major part of the detected angular broadening is related to the narrow diffraction pattern while the broad features in the spectra cause angular deflections on smaller scales. In this case the distance from the pulsar to the screen constitutes 2.5×10^{-3} of D , or about 5 pc (≈ 3 radii of the Crab nebula).

Now we will give some explanations on the technique of the measurement of the decorrelation bandwidth in the spectra of GPs. Since the intrinsic duration of GPs (τ_{GP}), after dispersion removal, is only a few microseconds, the frequency resolution in the radio spectra of GPs is restricted by the factor $1/\tau_{\text{GP}} \approx 0.3 - 3$ MHz. Prior to dedispersion, the smearing time over a 16-MHz band is equal to $660 \mu\text{s}$ giving a frequency resolution of 1.5 kHz but with low SNR. We chose to remove the dispersion only partly, corresponding to 80% of the DM value. This procedure leaves time smearing of $128 \mu\text{s}$ giving a frequency resolution of 7.8 kHz. With this approach power spectra were computed for all GPs with $\text{SNR} > 7\sigma$ (107 in total). Figure 2 (right) shows two different CCFs: the average CCF between power spectra of GPs recorded at LCP at Kalyazin and ARO, and the average CCF between power spectra of the same GPs recorded at Kalyazin at LCP and RCP. The approximation of these average CCFs with two gaussians gives values for the decorrelation bandwidths of 50 and 450 kHz. To estimate the characteristic time scale of scintillations we computed the average CCF between power spectra separated in time by a certain time lag. The narrow band feature in the CCF was only marginally detected at a level of about 2σ even for the closest GPs with a time separation less than 1 second.

Most interesting in Figure 2 (right) is the absence of any correlation between diffraction spectra of GP emission in LCP and RCP. In contrast, such correlation was found for B1937+21 (see Section 4.2). In the presence of a magnetic field the refractive indices of LCP and RCP waves are different. In principle, this can lead to different scattering for radio emission at LCP and RCP. However, the magnetic field strengths in the ISM (10^{-5} – 10^{-6} G) and in the Crab nebula (10^{-3} G) are too small to affect the scattering. We believe that the absence of correlation for the Crab pulsar could be caused in the region near the Crab pulsar where the low-frequency 33-Hz emission is converting to the pulsar wind. Just outside the light cylinder the magnetic field has a considerable tangential component of $\sim 10^6$ G, so the Larmour frequency, ν_H , is much larger than our observing frequency, ν , of 2244 MHz and remains larger up to distances of 30–50 light cylinder radii. The magnetic field does not have an effect on a linearly polarized wave of which the E-vector is parallel to the external H vector (ordinary wave). The refractive index is defined by the usual expression for a cold plasma. A wave with E-vector orthogonal to the external H-vector is an extraordinary wave. If $\nu_H \gg \nu$, then its refractive index is very close to 1, and the influence of the tangential magnetic field compensates almost completely the normal dispersion. The intensity of a circularly polarized wave has a periodic modulation with frequency. The intensity maxima of LCP coincide with the intensity minima of RCP and vice versa. This is likely the reason why the correlation between LCP and RCP scintillation fringes in the frequency domain is strongly suppressed at zero-lag but may rise at non-zero lag (~ 1 MHz). At a given frequency, ν , the period depends only on the column density number of free thermal electrons N_e : $P_\nu \approx 220D\nu^2/N_e$. Since $N_e \sim 4 \cdot 10^{15} \text{ cm}^{-3}$, it corresponds to a dispersion measure of $\sim 1.3 \cdot 10^{-3} \text{ pc cm}^{-3}$. This value is approximately equal to the range of variations of the dispersion measure observed for the Crab pulsar [10].

4. MEASUREMENTS OF PULSE SCATTERING OF THE PSR B1937+21

4.1. Data processing

Data processing was performed both at the Astro Space Center and York University (Toronto, Canada). Just after the observations, the raw data were split into separate pieces of 10^9 bytes and copied from the Mark5 '8-pack' disk modules to external 1-TB disks. Then these disks were shipped to the home institutions, and the Mark5 data were decoded and

the obtained signal was corrected for instantaneous bit statistics and amplitude bandpass irregularities and then coherently dedispersed. After dedispersion we were searching for giant pulses in every topocentric period with the detection threshold of 17σ in every 16-MHz band. The processing procedure and the detection criteria are described in detail in [11].

In 5.5 hours of pulsar data processed to date we found 6334 giant pulses stronger than 205 Jy in the 16-MHz bands. For further processing with the goal of studying GP scattering the 22 strongest GPs were selected which reached a peak flux density of > 1.2 kJy in the total 64-MHz band.

4.2. Decorrelation bandwidth and pulse broadening

Even observing at the relatively high frequency of 2100 MHz, the interstellar scattering of pulsar radio emission is still notable, especially when the signal is recorded with as high a time resolution as in our case. The scattering time, τ_{sc} , at our frequency may be estimated by extrapolating the scattering time measured at 1650 MHz [12]. Assuming $\tau_{sc} \sim \nu^{-4.4}$ (see Section 4.4) we obtain $\tau_{sc} \approx 40$ ns at our frequency or 5 samples for the total 64-MHz band. This value corresponds to a characteristic decorrelation bandwidth of ~ 4 MHz. First, to make accurate measurements of the decorrelation bandwidth and scattering time, we constructed the average ACFs and CCFs for the power spectra in LCP and RCP for the 22 selected strong GPs [see 11]. It should be mentioned, that in contrast to the VLBI observations of GPs from the Crab pulsar (see Section 3.2) the correlation between spectra in LCP and RCP for GPs from the B1937+21 is significant. Not only one, but two frequency scales of 3.79 ± 0.04 MHz and 16.5 ± 0.8 MHz were found [11].

To confirm the estimated scattering time of 40 ns, which is also derived from the measured decorrelation bandwidth of 3.8 MHz, we can also analyse directly GP shapes and measure their scattering time. To avoid random noise fluctuations of individual GPs, we fold together 20 GPs from the set we used for the CCF analysis dropping two GPs with relatively complex shapes that could be intrinsic to the pulses themselves rather than induced by the scattering in the ISM. This average profile of GPs is shown in Fig. 3. Fitting an exponential curve to the profile tail we obtained for the exponent $\tau_{sc} = 40 \pm 4$ ns which is the scattering time we could now assume for our observations at our observing frequency. It is evident that, when presenting the pulse profile with the flux density axis drawn in a logarithmic scale, the

exponential tail appears as a straight line. This line is clearly seen in the inset plot in Fig. 3. The measured slope gave us the broad-scale scattering time of $\tau_{\text{broad}} \approx 94 \pm 5$ ns that gives a corresponding decorrelation bandwidth of 1.7 ± 0.1 MHz.

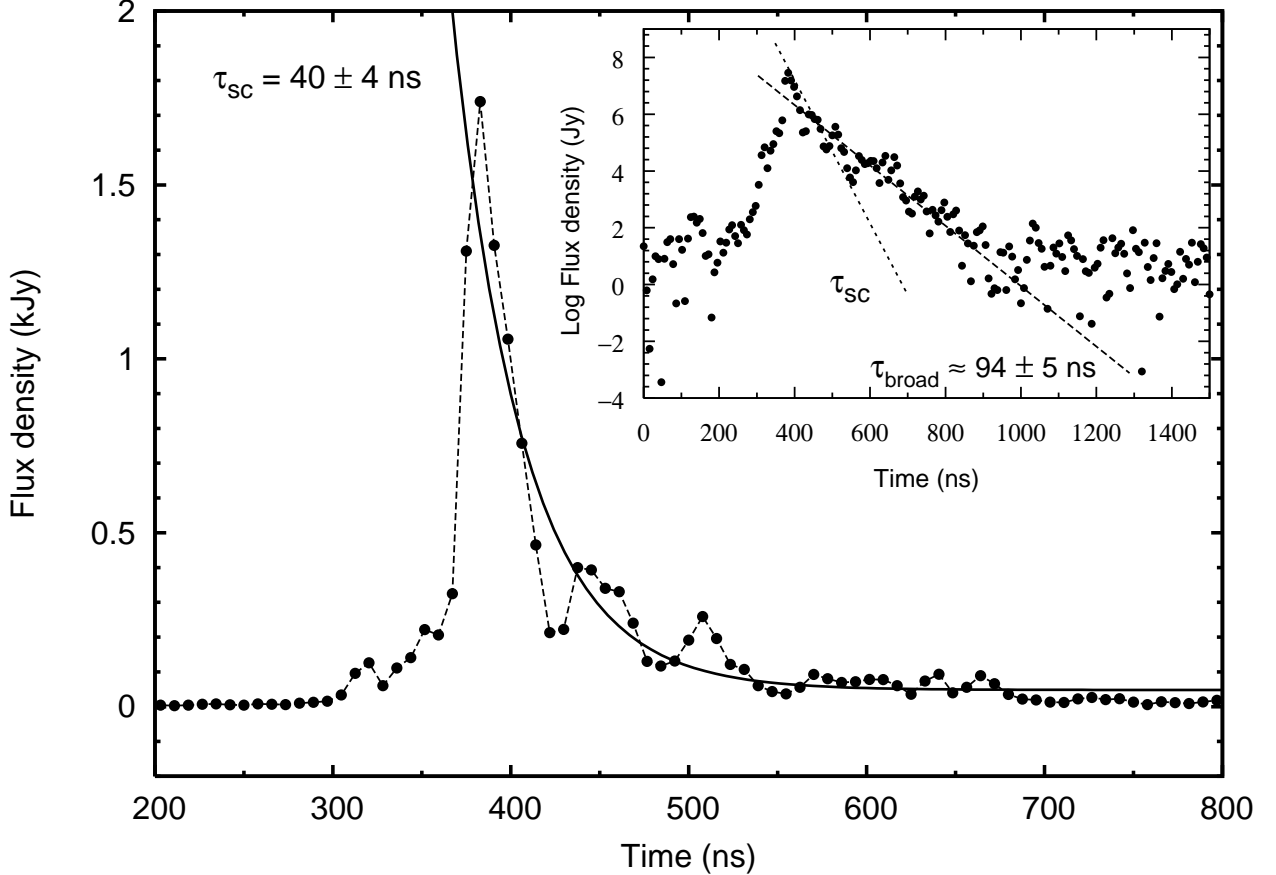


Figure 3. The average profile of 20 strong GPs of B1937+21 based on observations with the GBT at 2.1 GHz (dashed line). Solid line shows the least-square fit to the exponential scattering tail of the profile with an estimated scattering time $\tau_{\text{sc}} = 40 \pm 4$ ns. The inset plot represents the same GP average profile (points) in a larger time window and with the Y-axis drawn in logarithmic scale. The short-dashed line represents the fit from the main plot, and the long-dashed line is a least-square fit to the profile tail in logarithmic scale with a measured broad-scale scattering time $\tau_{\text{broad}} \approx 94 \pm 5$ ns.

Both main and inset plots are plotted with the sampling interval of 7.8125 ns.

Thus, analysing the power spectra and the average profile of GPs from B1937+21, we found three different frequency scales of 1.7, 3.8, and 16.5 MHz. It is likely that these scales correspond to different screens of enhanced interstellar plasma along the line of sight between the pulsar and Earth (spiral arms and the local screen).

4.3. Superresolution of giant pulses of the PSR B1937+21

As was concluded above, the width of giant pulses is affected by scattering. However, it turns out that in our particular case the ISM itself helps to put constraints on the intrinsic width of GPs. It is obvious that both regular and GPs travel along the same path and probe the same ISM. Thus, we can use the regular emission to correct the GP emission for the influence of the ISM. The apparent shape of the GPs is a result of convolution of the intrinsic GP waveform with the transfer function of the interstellar medium. We can use the diffraction spectrum obtained for regular emission as the transfer function to determine the intrinsic width of GPs by calculating the response on the infinitely short δ -pulse passed through a scattering medium.

Fortunately, the amplitude and the phase of the transfer function are not independent but related via the Hilbert transform [13, p. 553]. It allows us to obtain the waveform of the initially short but scattered pulse directly from the diffraction spectrum of the regular emission. In Fig. 4 the strongest GP is shown together with the simulated response from a δ -pulse. The comparison between the observed and simulated pulse shows very good agreement in the number of peaks, their relative amplitudes, and their positions. Such a good agreement is a strong evidence that the intrinsic width of GPs is less than our sampling interval of 8 ns.

This measured upper limit on the width of GPs allows us to put an upper limit on the size of the GP emitters in case GPs are temporal fluctuations. Then the size, d , of the giant pulse emitter, is $d < c\tau$, or less than 2 meters if relativistic effects can be ignored. Such a short duration together with the high peak flux density of 10 kJy gives a brightness temperature of the strongest GP of greater than 10^{37} K.

4.4. Frequency dependence of scattering time

Having measured the scattering parameters allows us to test the form of the spectrum of inhomogeneities of the electron density in the ISM. To do so we have to also use the measurements of the scattering time (or decorrelation bandwidth) at other frequencies. For B1937+21 we measured the scattering time to be 65 ns at 1650 MHz [12]. Cognard et al. [14] obtained the scattering time of 25 μ s at 430 MHz with observations at Arecibo. Kinkhabwala & Thorsett [15] put an upper limit for the scattering time of GPs at 1420 and 2380 MHz

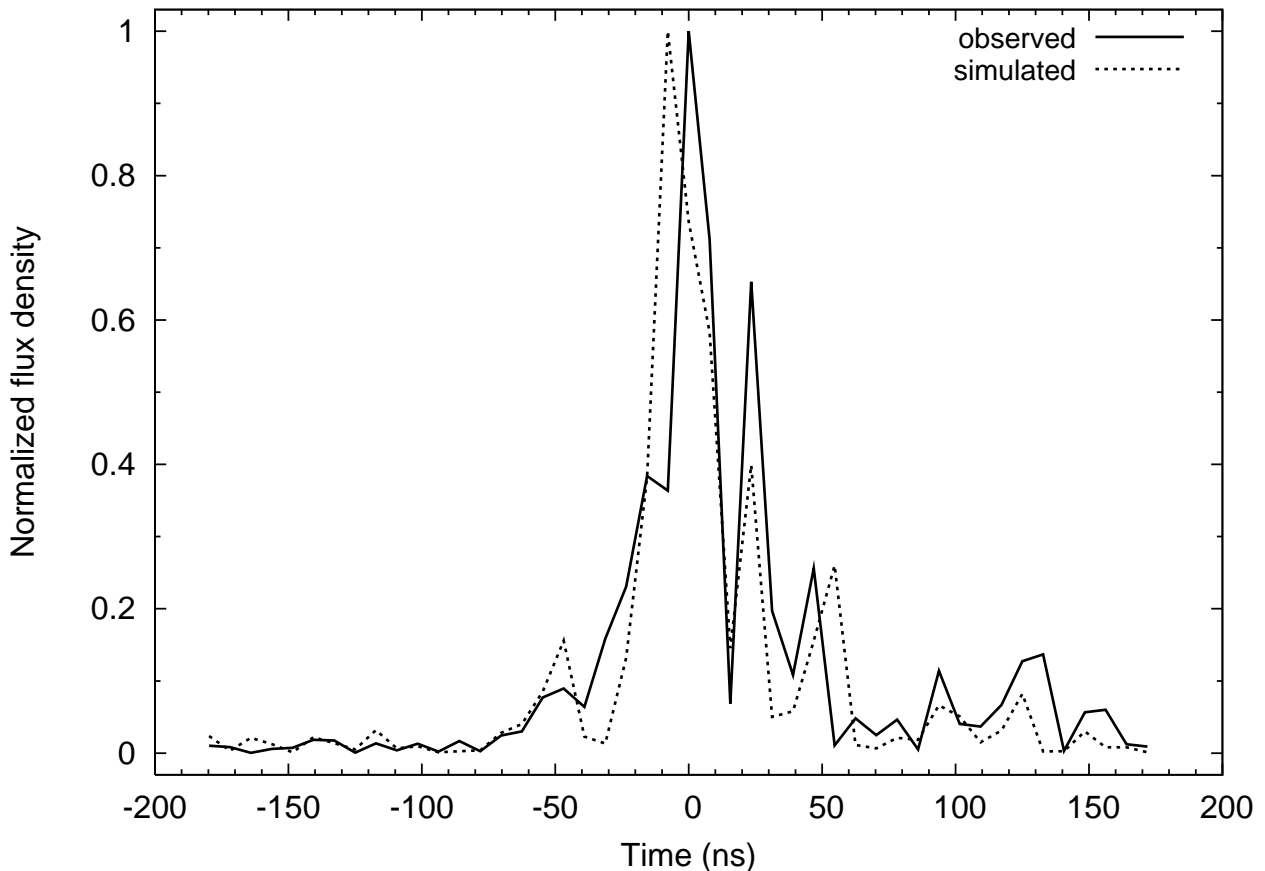


Figure 4. The strongest GP with a peak flux density of 10 kJy in the total 64-MHz band from B1937+21 recorded with the GBT at 2.1 GHz (solid line). The dashed line represents the simulated response from a δ -pulse passed through the ISM using the diffraction spectrum of regular emission as its transfer function. The observed and simulated pulses are shown with the sampling interval of 7.8125 ns.

to be 1.1 and 0.4 μ s, respectively. Fitting a power-law to these values results in an index of -4.2 ± 0.3 (see Fig. 5). This value for the index corresponds very well to the Kolmogorov spectrum of electron density.

For the Crab pulsar we used the values of scattering time obtained during the simultaneous observations of GPs at the frequencies of 23, 111, and 600 MHz [16] together with the measurement of the scattering time at 2244 MHz from our VLBI observation (see Section 3.2). These values of scattering time are: 3 s at 23 MHz, 15 ms at 111 MHz, 50 μ s at 600 MHz, and 0.2 μ s at 2244 MHz. These values together with a line representing the best fit are shown in Fig. 5. The measured power-law index is equal to -3.5 ± 0.1 which is

much lower than the value of -4.4 for the Kolmogorov spectrum, and even lower than -4 for the Gaussian spectrum. This lower value for the Crab pulsar may be due to the huge extra scattering in the surrounding Crab nebula.

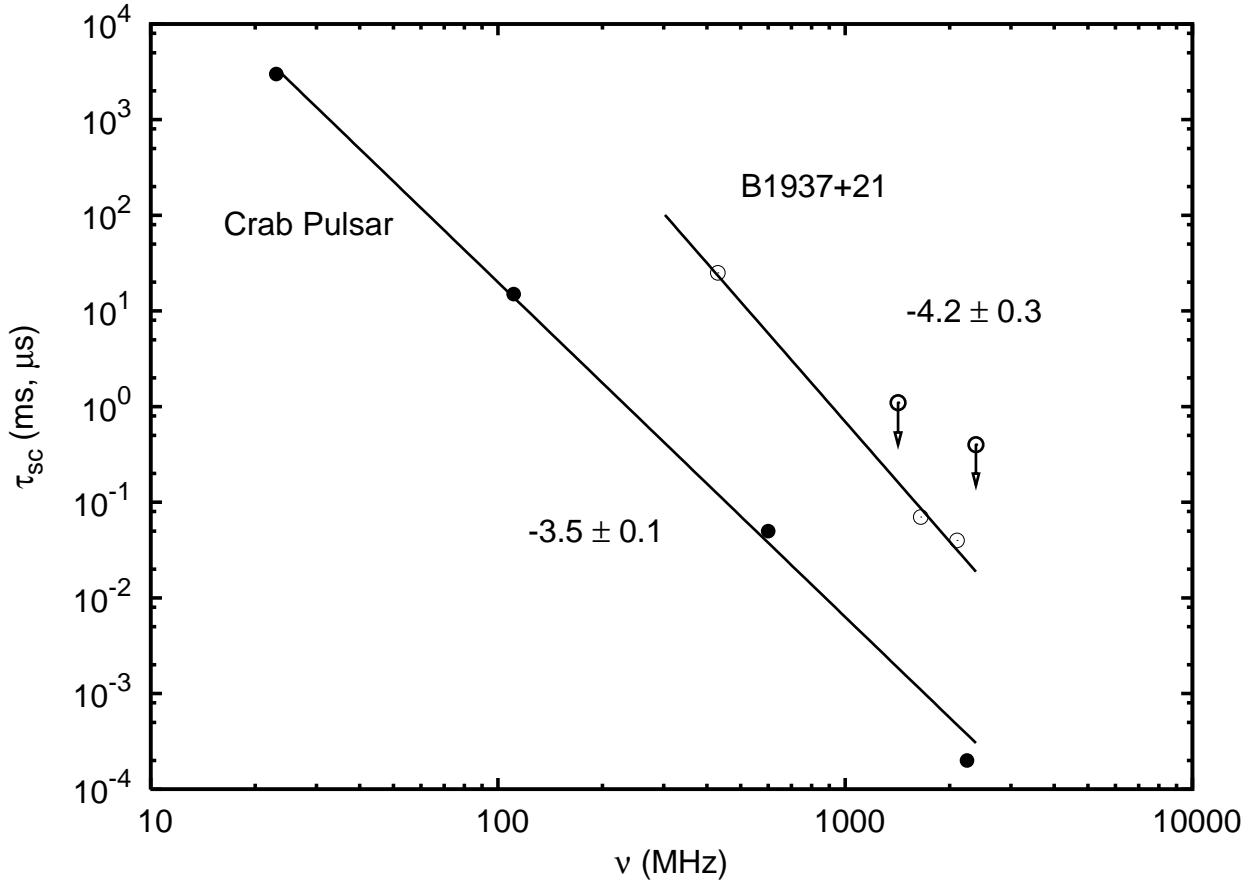


Figure 5. The frequency dependence of the scattering time, τ_{sc} , for B1937+21 (in μ s) and the Crab pulsar (in ms). The data points are from this paper and [12, 14–16] (for more detail, see text).

The solid lines represent least-squares power-law fits with indices of -4.2 ± 0.3 for B1937+21 and -3.5 ± 0.1 for the Crab pulsar.

5. CONCLUSIONS

Different frequency dependences of τ_{sc} were found for the millisecond pulsar and for the Crab pulsar with exponents of -4.2 ± 0.3 and -3.5 ± 0.1 , respectively. We attribute the difference to the notable influence of scattering in the Crab nebula. The location of the scattering region was estimated to be close to the outer edge of the Crab nebula. The estimate

is based on an analysis of the scattering diameter ($\theta_{sc} \approx 0.3$ mas), obtained through VLBI phase self-reference measurements, and the scattering time, determined from the diffraction pattern in radio spectra of GPs ($\Delta f = 50$ kHz). A significant difference was found between the diffraction pattern in radio spectra of GPs from the Crab pulsar emitted in RCP and LCP polarization channels. The effect is likely caused by the propagation of radio emission through the magnetized plasma of the Crab nebula. A simulation of the observed scattered waveform of GPs from B1937+21 has shown that the majority of GPs from this pulsar are shorter than 8 ns.

ACKNOWLEDGMENTS

We thank Frank Ghigo for extraordinary help in the preparation of the observations with the GBT and Konstantin Belousov and Andrey Chibisov for providing the operational S2-RDR play-back system. The Robert C. Byrd Green Bank Telescope (GBT) is operated by the National Radio Astronomy Observatory which is a facility of the U.S. National Science Foundation operated under cooperative agreement by Associated Universities, Inc. ARO is operated by the Geodetic Survey Division of Natural Resources Canada. VIK was a postdoctoral fellow at York University at the beginning of this project. Part of the project was done while YYK was a Jansky Fellow of the National Radio Astronomy Observatory and a research fellow of the Alexander von Humboldt Foundation. This project was supported in part by grants from the Canadian NSERC, the Russian Foundation for Basic Research (project number 07-02-00074) and the Presidium of the Russian Academy of Sciences “Origin and evolution of stars and galaxies”.

REFERENCES

1. Cannon, W. H., Baer, D., Feil, G., et al. 1997, *Vistas Astron.*, 41, 297
2. Kovalev, Y. Y., Ghigo, F., Kondratiev, V. I., et al. 2005, “Observing at the GBT with VLBA+Mark5A and VLBA+S2 backends”, GBT Commissioning Memo 236; available at http://wiki.gb.nrao.edu/pub/Knowledge/GBTMemos/GBT_Mark5A_S2.pdf

3. Krasinsky, G. A., & Vasilyev, M. V. 1997, in Proc. IAU Colloq. 165, Dynamics and Astrometry of Natural and Artificial Celestial Bodies, ed. I. M. Wytrzyszczak, J. H. Lieske, & R. A. Feldman (Dordrecht: Kluwer), 239
4. Jodrell Bank Crab Pulsar Monthly Ephemeris, <http://www.jb.man.ac.uk/~pulsar/crab.html>
5. Hankins, T. H. 1971, ApJ, 169, 487
6. Lorimer, D. R., & Kramer, M. 2005, Handbook of Pulsar Astronomy (Cambridge Univ. Press)
7. Cordes, J. M., Bhat, N. D. R., Hankins, T. H., et al. 2004, ApJ, 612, 375
8. Tompson, A. R., Moran, J. M., & Swenson, G. W. 1994, Interferometry and Synthesis in Radio Astronomy (John Wiley & Sons, Inc.)
9. Desai, K. M., Gwinn, C. R., Reynolds, J., et al. 1992, ApJ, 393, L75
10. Isaacman, R., & Rankin, J. M. 1977, ApJ, 214, 214
11. Kondratiev, V. I., Popov, M. V., Soglasnov, V. A., et al. 2006, in Proc. of the 363rd WE-Heraeus Seminar, Neutron Stars nad Pulsars. 40 years after the discovery, ed. W. Becker, & H. H. Huang, MPE Report 291, 24
12. Soglasnov, V. A., Popov, M. V., Bartel, N., et al. 2004, ApJ, 616, 439
13. Gonorovskii, I. S. 1977, Radio engineering circuits and signals (3rd ed.; Moscow: Izdatel'stvo Sovetskoe Radio)
14. Cognard, I., Shrauner, J. A., Taylor, J. H., & Thorsett, S. E. 1996, ApJ, 457, L81
15. Kinkhabwala, A., & Thorsett, S. E. 2000, ApJ, 535, 365
16. Popov, M. V., Kuzmin, A. D., Ulyanov, O. V., et al. 2006, ARep, 50, 562, transl. from: AZh, 2006, 83, 630